Chemosphere 184 (2017) 127–136

Contents lists available at ScienceDirect

Chemosphere

journal homepage: www.elsevier.com/locate/chemosphere

Interactions of carbon nanotubes and/or graphene with manganese peroxidase during biodegradation of endocrine disruptors and triclosan

Ming Chen [a, b], Guangming Zeng [a, b, *], Cui Lai [a, b, **], Chang Zhang [a, b], Piao Xu [a, b], Min Yan [a, b], Weiping Xiong [a, b]

[a] College of Environmental Science and Engineering, Hunan University, Changsha 410082, China
[b] Key Laboratory of Environmental Biology and Pollution Control (Hunan University), Ministry of Education, Changsha 410082, China

HIGHLIGHTS

- GRA, SWCNT or SWCNT+GRA had different impacts on the overall binding stability between MnP and its substrates during biodegradation of EDs and personal care products.
- GRA, SWCNT or SWCNT+GRA changed the number and behavior of water molecules adjacent to both MnP and its substrates.
- Some sensitive residues from MnP to disturbance of GRA, SWCNT or SWCNT+GRA were found.

ARTICLE INFO

Article history:
Received 28 November 2016
Received in revised form
8 May 2017
Accepted 29 May 2017
Available online 29 May 2017

Handling Editor: Chang-Ping Yu

Keywords:
Carbon nanotube
Graphene
Biodegradation
Endocrine disruptors
Personal care products

ABSTRACT

Molecular-level biodegradation processes of bisphenol A (BPA), nonylphenol (NP) and triclosan (TCS) mediated by manganese peroxidase (MnP) were investigated with and without single-walled carbon nanotube (SWCNT) and/or graphene (GRA). Although the incorporation of SWCNT, GRA or their combination (SWCNT+GRA) did not break up the complexes composed of manganese peroxidase (MnP) and these substrates, they had different effects on the native contacts between the substrates and MnP. GRA tended to decrease the overall stability of the binding between MnP and its substrates. SWCNT or SWCNT+GRA generally had a minor impact on the mean binding energy between MnP and its substrates. We detected some sensitive residues from MnP that were dramatically disturbed by the GRA, SWCNT or SWCNT+GRA. Nanomaterials changed the number and behavior of water molecules adjacent to both MnP and its substrates, which was not due to the destruction of H-bond network formed by sensitive regions and water molecules. The present results are useful for understanding the molecular basis of pollutant biodegradation affected by the nanomaterials in the environment, and are also helpful in assessing the risks of these materials to the environment.

1. Introduction

The extensive use of carbon nanotubes (CNTs), graphene (GRA) and other nanomaterials has been resulting in their release into the environment and increasing the exposure of living organisms to these materials (Zhang et al., 2007; Gong et al., 2009; Feng et al., 2010; Xu et al., 2012; Kotchey et al., 2013; Zhao et al., 2014; Chen et al., 2016b). There is evidence that these materials presented toxic effects on environmental microbes (Akhavan and Ghaderi, 2010; Rodrigues et al., 2013; Xie et al., 2016). Moreover, enzymatic immobilization onto carbon nanomaterials can change enzymatic activity (Mubarak et al., 2014; Hermanová et al., 2015). These previous findings suggest that nanomaterials release may affect the biodegradation processes of common contaminants such as endocrine disruptors (EDs) and personal care products in the environment.

EDs and personal care products are emerging as persistent contaminants, and were often detected together in wastewater

* Corresponding author. College of Environmental Science and Engineering, Hunan University, Changsha 410082, China.
** Corresponding author. College of Environmental Science and Engineering, Hunan University, Changsha 410082, China.
E-mail addresses: zgming@hnu.edu.cn (G. Zeng), laicui888@163.com (C. Lai).

http://dx.doi.org/10.1016/j.chemosphere.2017.05.162
0045-6535/

(Kasprzyk-Hordern et al., 2009). ED is a group of chemicals that may disrupt or modulate the endocrine system of human and other living organisms (Cabana et al., 2007b). Bisphenol A (BPA) and nonylphenol (NP) are two typical EDs, which have been extensively found in the environment due to increasing use of the products that contain these EDs (Cajthaml, 2015). Thus, BPA and NP are often selected as representatives for the EDs' biodegradation studies (Cabana et al., 2007a). BPA is known to be the material for producing phenol resins, epoxy resins, food packaging coat, *etc*, exhibiting toxic effects on aquatic organisms (Kang et al., 2006). NP not only could adsorb to sediments/particles, but also could accumulate in biological tissues (Uguz et al., 2003; Korsman et al., 2015; Vidal-Liñán et al., 2015). In addition to these well-known EDs, it has been demonstrated that triclosan (TCS), a preservative and antimicrobial agent that is extensively applied in the personal care products, was thought to have potential estrogenic activity.

A lot of studies have found that EDs and TCS could be degraded by white rot fungi. It was shown that *P. chrysosporium* was versatile because it could degrade a wide range of substrates, including BPA, NP, TCS, *etc* (Tsutsumi et al., 2001; Huang et al., 2008). Another versatile microorganism was *Trametes versicolor* which also decomposed various EDs and TCS (Hundt et al., 2000; Takamiya et al., 2008). Other microbes were also observed to have the ability to metabolize EDs and TCS. For example, *Pleurotus ostreatus* reduced about 80% of BPA within 12 days (Hirano et al., 2000). Their abilities to degrade EDs and TCS are derived from their secreted ligninolytic enzymes. Among these enzymes, MnP and laccase are extensively investigated for their performance in the biodegradation of EDs and TCS. BPA and NP were removed by *P. chrysosporium* MnP within 1 h, but their estrogenic activities were still kept partly after 1–3 h (Tsutsumi et al., 2001). These reactions were performed in the mixtures containing BPA or NP, MnP, malonate buffer (pH = 4.5), glucose oxidase, glucose, and $MnSO_4$ at 30 °C. *P. ostreatus* MnP could degrade BPA, and convert it to phenol, hexestrol, 4-isopropylphenol and 4-isopropenylphenol (Hirano et al., 2000). Laccase extracted from *Coriolopsis polyzona* was found to simultaneously eliminate BPA, NP and TCS (Cabana et al., 2007a). *T. versicolor* laccase could catalyze the conversion of BPA and NP (Kim and Nicell, 2006; Kim et al., 2008). Inoue et al. (2010) found that *P. chrysosporium* MnP eliminated about 94% of TCS after half an hour and almost 100% of TCS after 1 h.

Molecular dynamics (MD) simulations have proved successful in understanding the biodegradation processes at the atomic level (Chen et al., 2017a, 2017b). Awasthi et al. (2015) employed molecular docking, MD simulations and binding free energy calculation to explain the functional difference between fungal and plant laccases (*i.e*., fungal laccases tended to degrade lignin, while plant laccases preferred to synthesize lignin). MD investigation carried out by us on the *T. versicolor* laccase in complex with ferulic acid, 2,6-dimethoxyphenol, sinapic acid, vanillyl alcohol and guaiacol has given the insight into their interactional processes during biodegradation (Chen et al., 2015b). We found that hydrophobic interactions rather than H-bonds were necessary to the interaction of laccase with these lignin model compounds. It was reported that Trp residue and its π-Cation interaction with substrate were key to degrade 2, 4, 6-trinitrotoluene based on MD simulation results (Bhattacherjee et al., 2014).

Up to now, the biodegrading processes of EDs and personal care products have not yet been well examined in the presence of GRA and/or SWCNT in the environment at the molecular level, although a wide variety of studies have focused on their respective environmental and ecological impacts (Zhang et al., 2010). The objective of this study was to explore the interactions of CNTs and/or GRA with MnP during biodegradation of endocrine disruptors and triclosan.

2. Materials and methods

2.1. Endocrine disruptors and TCS

In this study, two EDs (BPA and NP) and a personal care product (TCS) were selected. Their chemical structures were obtained from ChemSpider (Pence and Williams, 2010) in the 3D mol format. Their properties were from ChemSpider, PubChem (Kim et al., 2015) or published literature, and are shown in Table 1. In cases where multiple values for water solubility, Log Kow or pKa were given, only one value was adopted for each of them.

2.2. MnP from phanerochaete chrysosporium

There are multiple experiment-determined 3D structures of *P. chrysosporium* MnP available in PDB (Rose et al., 2013). Based on our research purpose, we selected the substrate-free MnP (PDB code: 1YZP) (Sundaramoorthy et al., 2005). This structure is at a resolution of 1.6 Å with a total structure weight of 38,876.59. The MnP is composed of 357 amino acids.

2.3. Complexes

Initial conformations of GRA and/or SWCNT binding to MnP were created by PatchDock (Schneidman-Duhovny et al., 2005) and FireDock (Mashiach et al., 2008), as described previously by us (Chen et al., 2016a). Complexes of BPA, NP and TCS with MnP were constructed using Molegro Virtual Docker (MVD) (Thomsen and Christensen, 2006), following our previous methods (Chen et al., 2015b), respectively. Finally, a total of 12 complexes were produced (Fig. 1): BPA-MnP, BPA-GRA- MnP, BPA-SWCNT-MnP, BPA-SWCNT-GRA-MnP, NP-MnP, NP-GRA-MnP, NP-SWCNT-MnP, NP-SWCNT-GRA-MnP, TCS-MnP, TCS-GRA-MnP, TCS-SWCNT-MnP and TCS-SWCNT-GRA-MnP.

2.4. MD simulations

Gromacs 4.6 software (Hess et al., 2008), an extensively used MD simulation software, was employed for the present study, taking OPLS/AA force filed (Kaminski et al., 2001) into consideration. This force field has been reported to have an excellent performance for the simulations of nanomaterials, organic molecules and enzymes (Chen et al., 2016b). For each substrate binding to MnP, four systems were constructed, one with SWCNT, one with GRA, one with these two types of nanomaterials and one without them. All these systems were put under the same conditions for the MD simulations to facilitate their comparison. A total of 12 systems were constructed (Fig. 1). For each system, 500-ps NVT+500-ps NPT+50-ns MD simulations were carried out. Thus, a total of 612 ns were run.

Table 1
Properties of BPA, NP and TCS.

Properties	BPA	NP	TCS
Chemical formula	$C_{15}H_{16}O_2$	$C_{15}H_{24}O$	$C_{12}H_7Cl_3O_2$
Molecular weight	228.291 g/mol	220.356 g/mol	289.536 g/mol
Water solubility	120 mg/L	6 mg/L	10 mg/L
Log Kow	3.32	5.76	4.76
pKa	9.6	10.7[a]	7.9

[a] p*Ka* value is from Vazquez-Duhalt et al. (2005). Other values are from ChemSpider or PubChem.

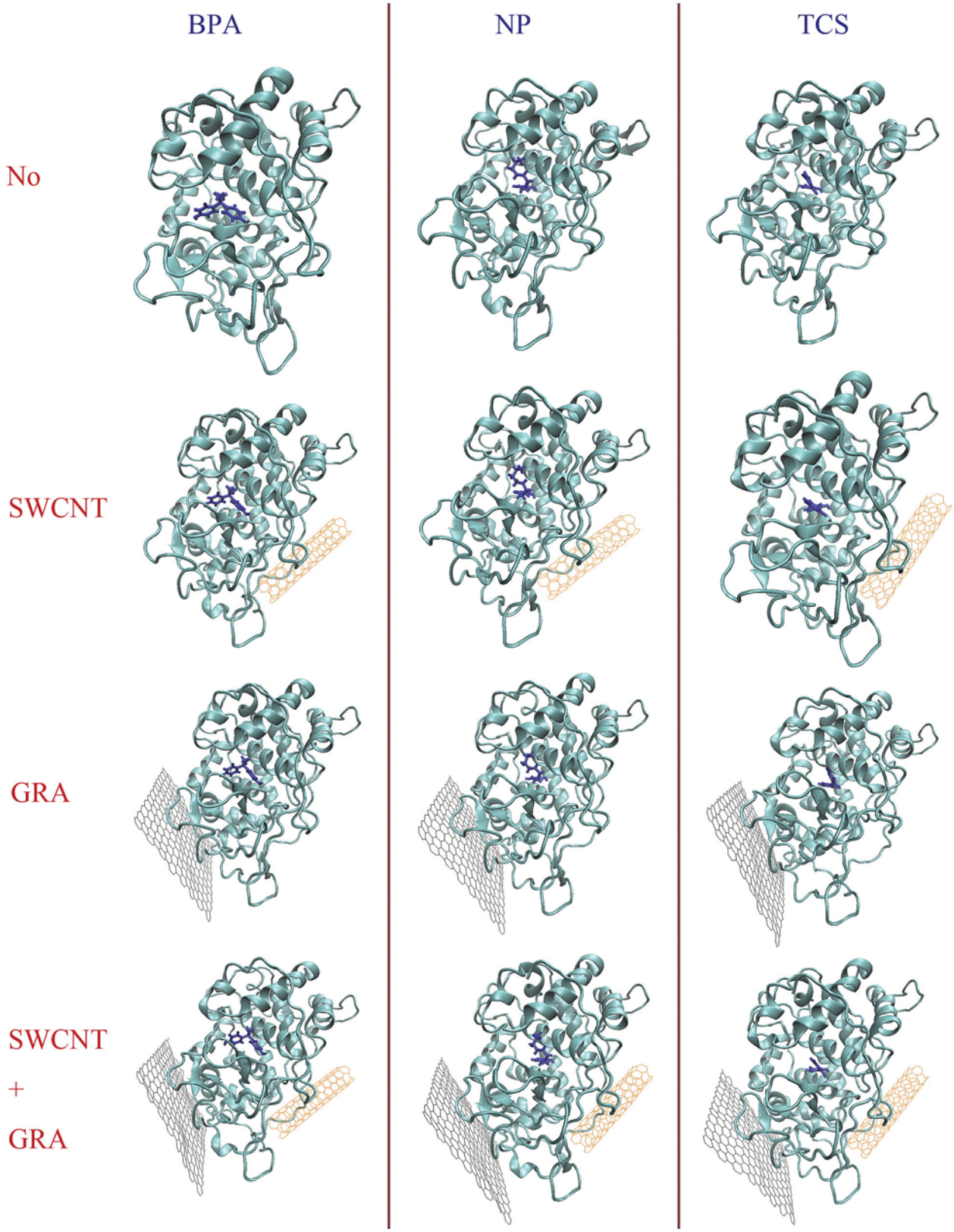

Fig. 1. The initial conformations of BPA, NP and TCS with MnP in the absence and presence of nanomaterials at 0 ns. "No" shows that no nanomaterials are presented; "SWCNT", "GRA" and "SWCNT+GRA" shows that only SWCNT, only GRA and both SWCNT and GRA are presented, respectively. The substrates are in blue.

2.5. Binding free-energy calculation

The tool g_mmpbsa (Kumari et al., 2014) relying on the mechanics/Poisson-Boltzmann Surface Area (MM/PBSA) method was employed to calculate the binding free energies between MnP and various substrates with and without SWCNT and/or GRA for the last 10 ns. A total of 200 snapshots for each trajectory at an interval of 50 ps were saved for this calculation where van der Waal energy, electrostatic energy, polar solvation energy and solvent accessible surface area (SASA) energy were considered. We not only calculated the average binding energies for each complex, but also analyzed the contribution energies of individual residues.

2.6. Water molecules dynamics

We counted the water number within 5 Å of MnP and within 5 Å of ligands (BPA, NP or TCS) for the last 10 ns at an interval of 50 ps by performing a tcl code in VMD (Humphrey et al., 1996) that was used in our previous study (Chen et al., 2016b). Moreover, we also investigated the H-bond network between water molecules and sensitive regions by counting the H-bond number between them during the whole simulation.

3. Results and discussion

EDs and personal care products extensively exist in the environment with high bioavailability and potentially adverse ecological and health effects, requiring a reliable approach to remove them (Kasprzyk-Hordern et al., 2009; Cajthaml, 2015). Biodegradation technology is a common way to accomplish this goal. However, EDs' biodegradability of microbes was limited by many factors such as temperature and pH (Kim and Nicell, 2006; Cabana et al., 2007a). Nanomaterials such as GRA and SWCNT are released into the environment due to human factors and then causing environmental issues. In particular, the appearance of nanomaterials in the environment may become a new factor that influences the biodegradation of EDs and personal care products.

We only selected the microbial enzyme (i.e. *P. chrysosporium* MnP) for the present purpose. *P. chrysosporium* MnP belongs to heme peroxidase, catalyzing the oxidation of phenolic substrates relying on H_2O_2 and Mn (II) (Sundaramoorthy et al., 2010). The reason we selected microbial enzyme was that investigating microbial degradation of EDs and personal care products was helpful in the industrial applications and environmental protection, because microbial degradation has been extensively used in practical applications and easily operated. For example, in wastewater

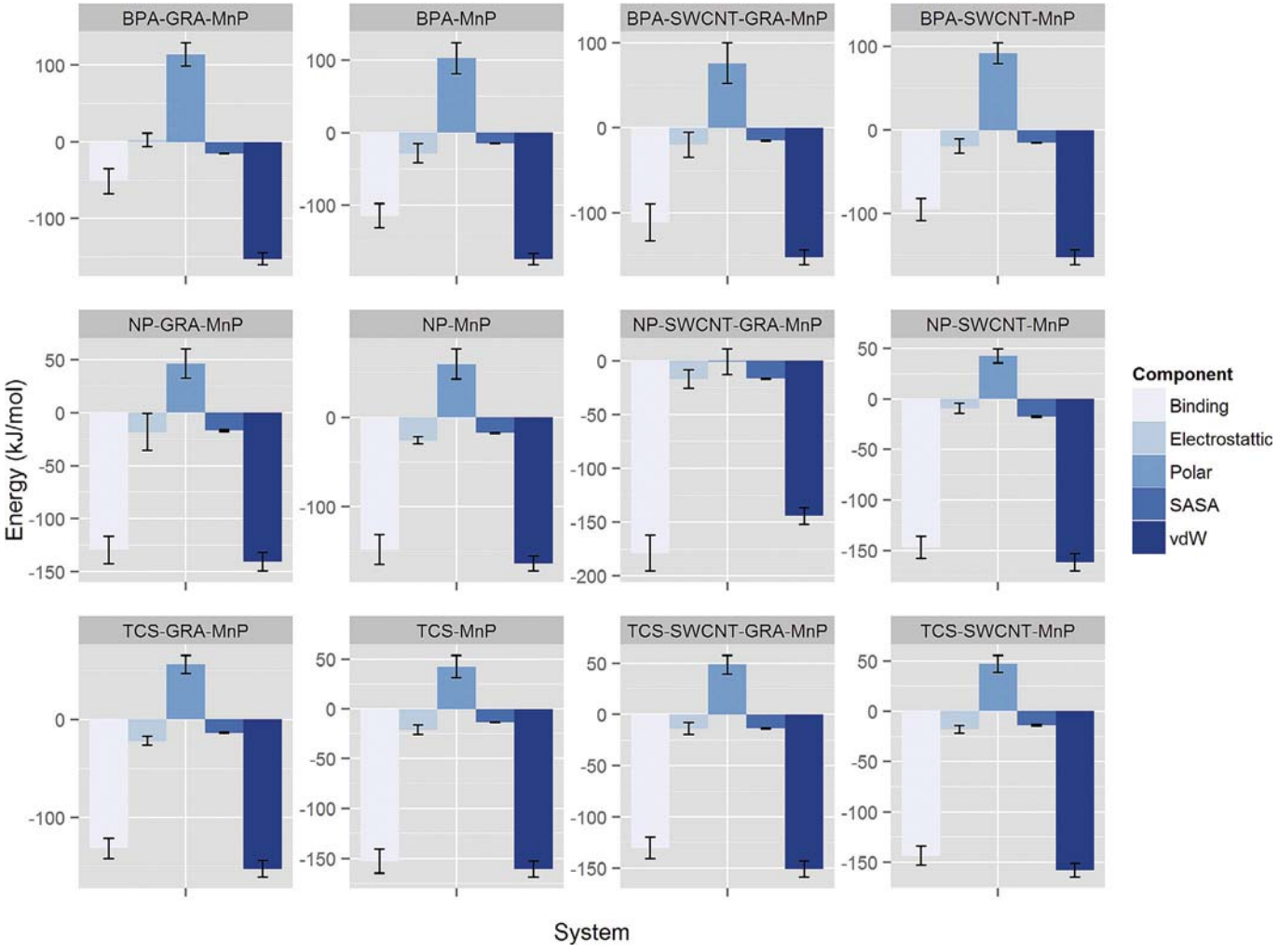

Fig. 2. Binding energies for the substrates (BPA, NP or TCS) complexed with MnP.

treatment plants, microbial degradation has proved to be an efficient method to remove EDs from waste water (Fürhacker et al., 2000). Moreover, *P. chrysosporium* is the best studied white rot fungi that produce the ligninolytic enzymes (Inoue et al., 2010; Chen et al., 2015a; Zhao et al., 2015). The most important reason for this selection was that *P. chrysosporium* MnP was effective in removing all analyzed substrates in this study (i.e. BPA, NP and TCS) (Tsutsumi et al., 2001; Inoue et al., 2010).

The initial conformations of BPA, NP and TCS with MnP in the absence and presence of nanomaterials at 0 ns was shown in Fig. 1. Our results elucidated the facts that the incorporation of nanomaterials would change the binding conformations of BPA, NP and TCS to MnP, and thus would affect their biodegradation processes.

3.1. Binding-energy variations caused by SWCNT and/or GRA

Binding energy is an important parameter for assessing the binding stability of a receptor to a ligand (Anwar et al., 2015). Thus, we determined the binding free-energy between MnP and three analyzed substrates (BPA, NP and TCS) using MM/PBSA method (Kumari et al., 2014). This method has been extensively applied to calculate the binding energy in a variety of systems (Anwar et al., 2015; Awasthi et al., 2015; Omotuyi, 2015). In a previous article, it was demonstrated that van der Waals (vdW) interactions were the driving force of lysozyme bound to CNT (Calvaresi et al., 2012). Moreover, Awasthi et al. (2015) reported that vdW interactions were the main factor that contributed to the binding of lignin model compounds to fungal and plant laccases. The analyses of energy components from our study also indicated that vdW interactions were the most important driving force for the binding between MnP and its substrates in all surveyed complexes during biodegradation. It must be noted that the binding energy in this study always refers to the one between MnP and its substrates (BPA, NP or TCS). Mean binding energy between MnP and BPA was higher than that between MnP and NP or between MnP and TCS in the presence or absence of nanomaterials (Fig. 2).

MnP not only is able to degrade BPA, but also is capable of eliminating BPA's estrogenic activity. This paper provided a critical insight into the molecular mechanism involved in the impact of GRA and/or SWCNT on binding energy between BPA and MnP. The combination of SWCNT and GRA slightly reduced the binding stability of BPA to MnP with a mean binding energy of −111.423 ± 21.810 kJ/mol which was larger than that in the

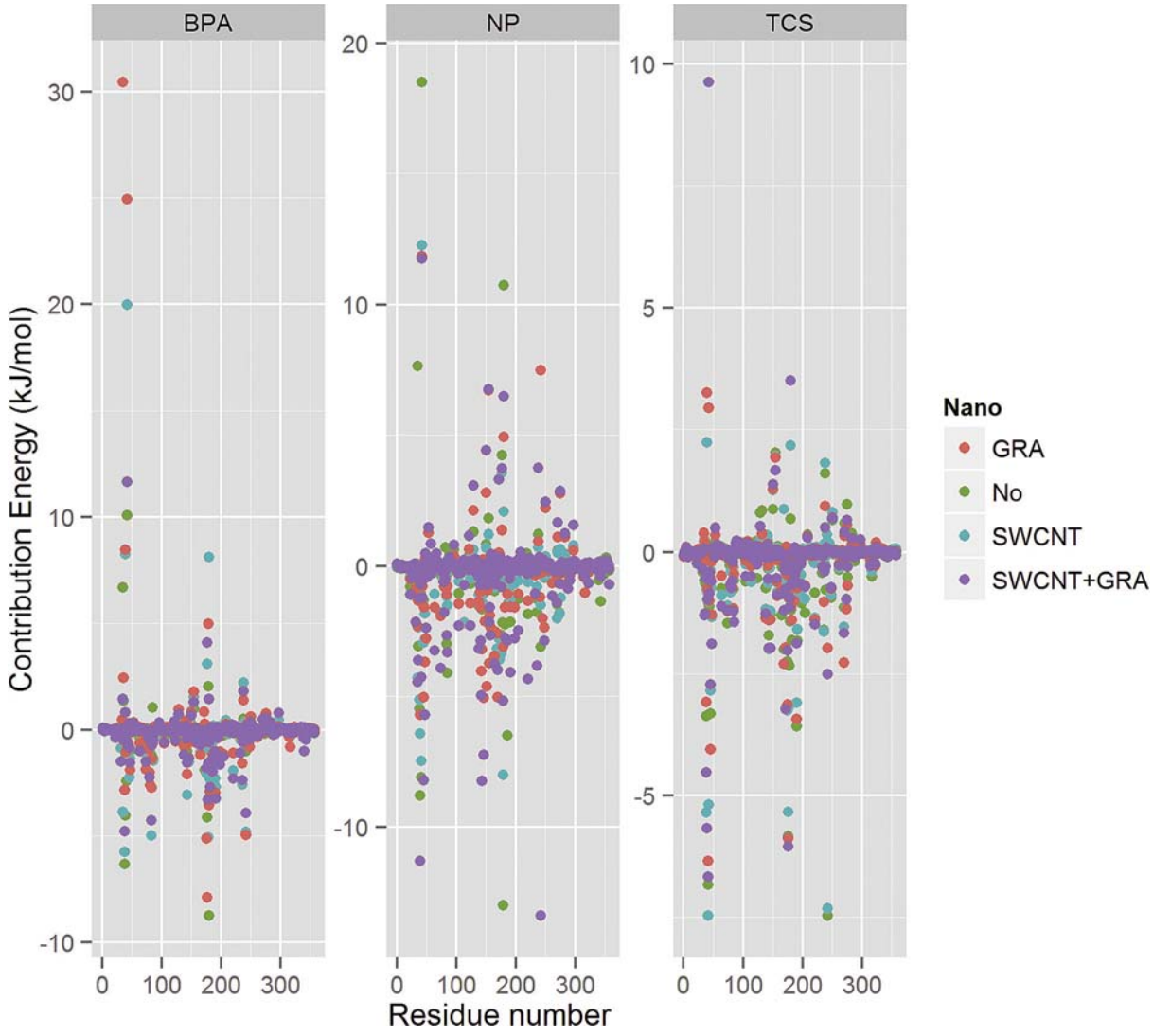

Fig. 3. Contribution energy of each residue to total binding energy. "No" shows that no nanomaterials are presented; "SWCNT", "GRA" and "SWCNT+GRA" shows that only SWCNT, only GRA and both SWCNT and GRA are presented, respectively.

absence of nanomaterials (−114.746 ± 16.857 kJ/mol). Also, the separate impact of SWCNT on the binding of BPA to MnP was small. Interestingly, GRA significantly affected the binding energy of BPA to MnP, increasing the binding energy by about half as compared to that without nanomaterials (−51.558 ± 16.731 kJ/mol vs. −114.746 ± 16.857 kJ/mol). These findings suggested that the presence of SWCNT could mitigate the strong effect of GRA on the binding of BPA to MnP during biodegradation to a certain extent.

It is very critical to clearly reveal the process how GRA and/or SWCNT affect the NP biodegradation to optimize this process, because the NP-degrading microbes or enzymes may be exposed to these nanomaterials during NP biodegradation. Mean binding energy is −147.796 ± 16.480 kJ/mol, −146.883 ± 11.073 kJ/mol, −129.716 ± 13.047 kJ/mol, −178.843 ± 16.723 kJ/mol for NP-MNP, NP-SWCNT-MNP, NP-GRA-MNP and NP-SWCNT-GRA-MNP, respectively. Obviously, single GRA or SWCNT tended to decrease the binding stability of NP to MnP, while their combination preferred to enhance the stability.

TCS-SWCNT-MNP had a binding energy of −9.621 kJ/mol lesser than that of TCS-MNP (−153.091 kJ/mol vs. −143.47 kJ/mol). In comparison to SWCNT, a larger difference in the binding energy was observed between TCS-GRA-MNP and TCS-MNP (−21.418 kJ/mol). In particular, this difference was similar to that between TCS-SWCNT-GRA-MNP and TCS-MNP (−22.84 kJ/mol). These results implied that SWCNT had fewer effects on the binding energy of TCS to MnP than GRA. Thus, SWCNT and GRA had distinctive impacts on the binding energies between MnP and its substrates during biodegradation. This may be due to their different properties such as the shape (rolled for SWCNT and planar for GRA), surface area, *etc*. The shape has been found to play an important role in nanomaterials-induced cytotoxic effects (Zhang et al., 2010). Besides, a previous study observed that several amino acids exhibited weaker binding strength with SWCNT than with GRA (Rajesh et al., 2009). The weaker binding strength between SWCNT and amino acid residues might be also the reason that SWCNT generally had few effects on the binding between MnP and its substrates than GRA. Their combination led to a relatively moderate change in the binding energies.

3.2. Sensitive residues

We further identified the contribution of each residue to the total binding energy by the MM-PBSA method (Kumari et al., 2014). Some previous studies also performed the energy-decomposing work to determine which residues had the largest contributions to the binding energy (Zoete et al., 2005; Calvaresi et al., 2012). Contribution energy of individual residues was shown in Fig. 3. Overall, residues of MnP to NP and TCS were more easily affected by nanomaterials than those bound to BPA. We found some residues were largely disturbed by SWCNT, GRA or their combination. We called these residues “sensitive residues”. In this study, sensitive residues were identified by the following formula:

$$R = \begin{cases} 1 & if\ D1 \geq 4\,kJ/mol \text{ or } D2 \geq 4\,kJ/mol \text{ or } D3 \geq 4\,kJ/mol \\ 0 \end{cases}$$

$$D1 = |E - E_{SWCNT}|$$

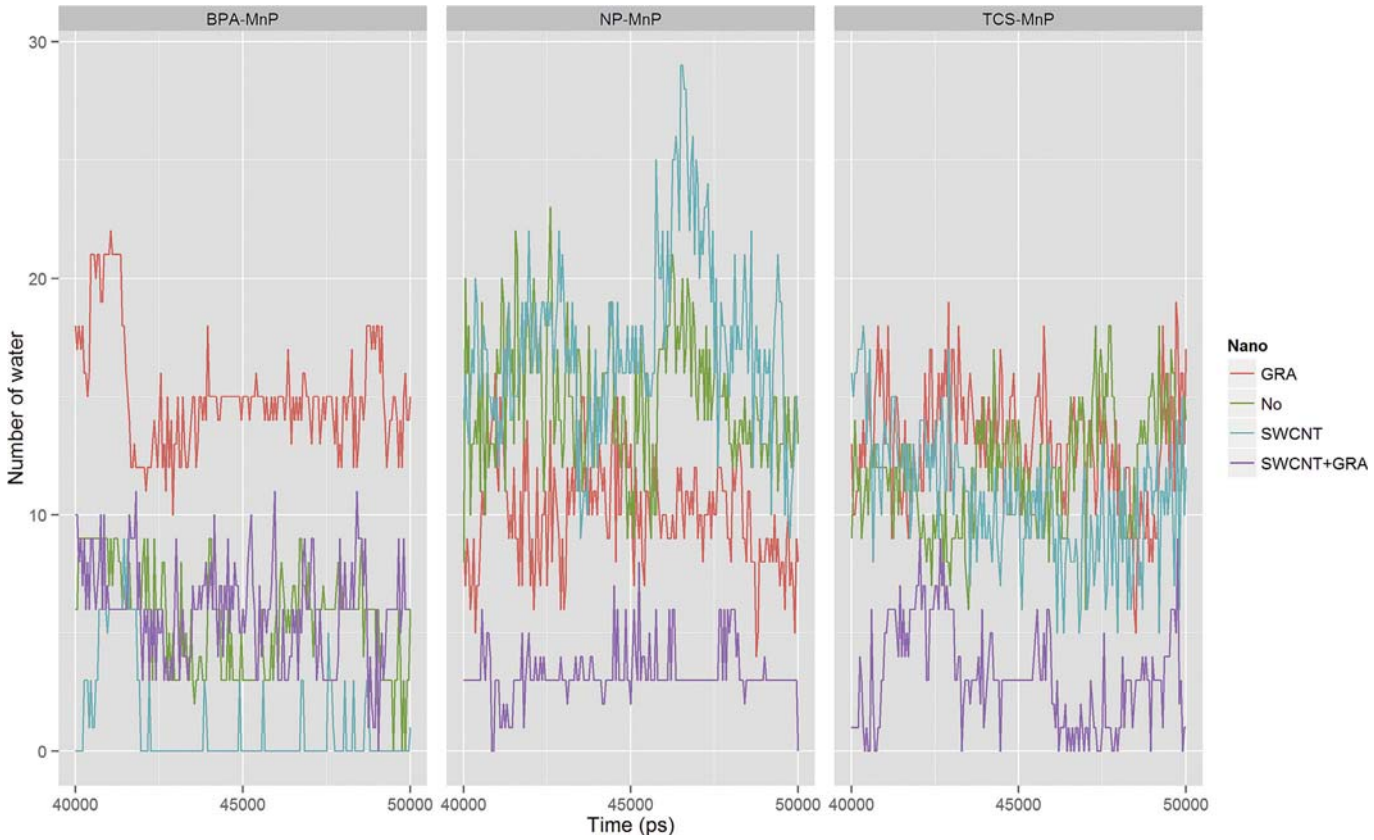

Fig. 4. Water number within 5 Å of MnP and within 5 Å of ligands (BPA, NP or TCS). “No” shows that no nanomaterials are presented; “SWCNT”, “GRA” and “SWCNT+GRA” shows that only SWCNT, only GRA and both SWCNT and GRA are presented, respectively.

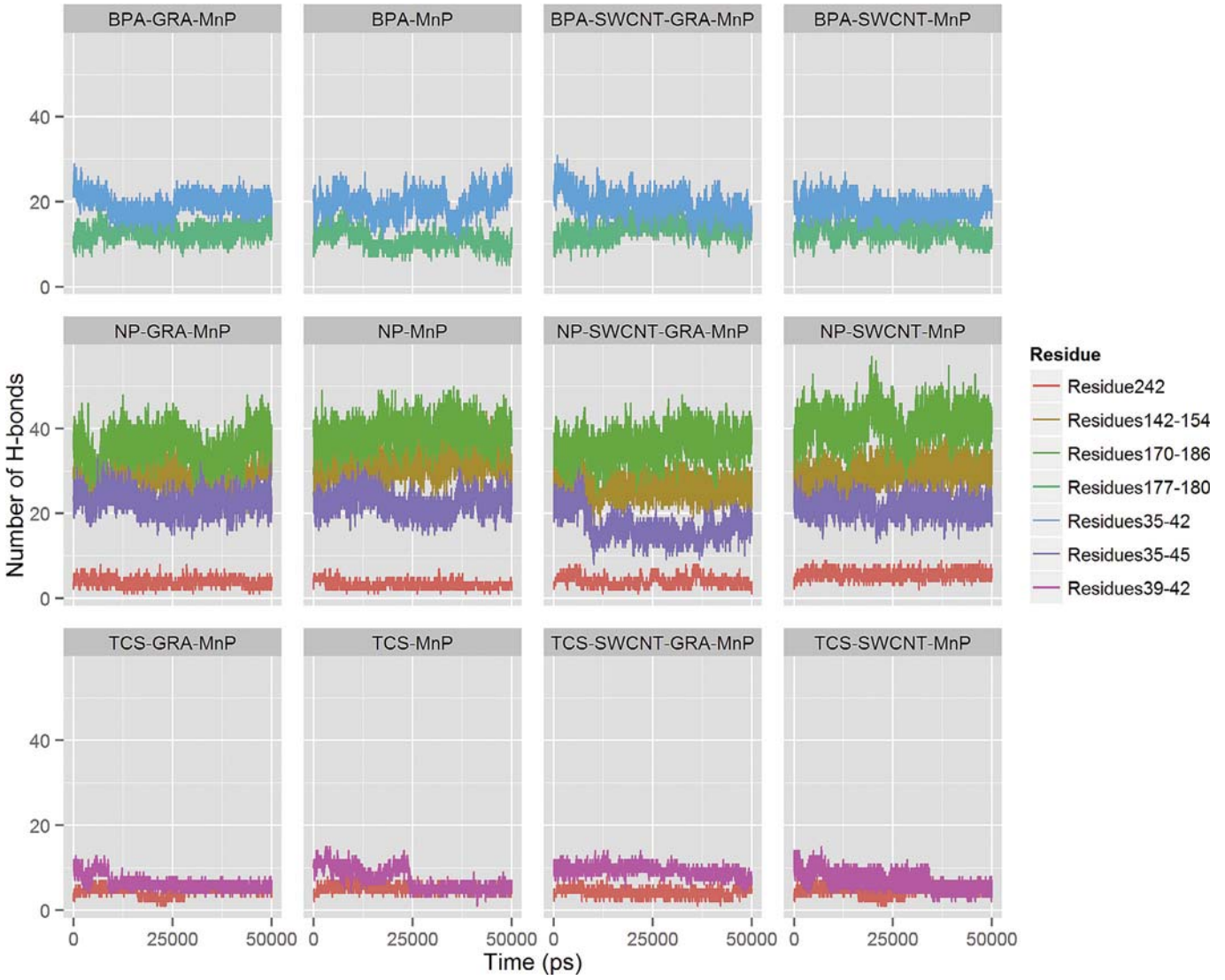

Fig. 5. H-bond contacts of sensitive regions with water molecules with and without nanomaterials.

$$D2 = |E - E_{GRA}|$$

$$D3 = |E - E_{SWCNT+GRA}|$$

where R is the indicator of a sensitive residue, the value "1" shows the residue is a sensitive residue; E is the contribution energy of the residue in the absence of nanomaterials; E_{SWCNT}, E_{GRA} and $E_{SWCNT+GRA}$ are the contribution energy of the residue for SWCNT, GRA and their combination, respectively; D1 is the absolute value of the difference between E and E_{SWCNT}; D2 is the absolute value of the difference between E and E_{GRA}; D3 is the absolute value of the difference between E and $E_{SWCNT+GRA}$. The energy value "4 kJ/mol" was manually selected to determine the sensitive residues based on a careful observation on the trend of contribution energy variation.

Six residues from MnP bound to BPA (residues 35, 39, 42, 177, 179 and 180), 16 residues from MnP complexed with NP (35, 38, 41, 42, 45, 142, 143, 146, 151, 154, 170, 172, 179, 180, 186 and 242), and three residues from MnP bound to TCS (39, 42 and 242) were found to be sensitive residues. These residues had a dominant role in changing the binding energy. In case of BPA, the energy change caused by SWCNT, GRA and their combination was 10.5774 kJ/mol, 23.7591 kJ/mol and 5.2484 kJ/mol for residue 35, 12.3162 kJ/mol, 12.5163 kJ/mol and 4.862 kJ/mol for residue 39, 9.912 kJ/mol, 14.88773 kJ/mol and 1.5568 kJ/mol for residue 42, 7.2287 kJ/mol, 3.7827 kJ/mol and 8.2166 kJ/mol for residue 177, 7.1086 kJ/mol, 2.9388 kJ/mol and 3.6231 kJ/mol for residue 179, and 16.8964 kJ/mol, 5.2029 kJ/mol and 10.2095 kJ/mol for reisude 180. In gereral, single SWCNT or GRA had larger effects on the contribution energy of sensitive residues from the BPA-MNP, while thier combination was helpful in reducing the contribution-energy fluctuations of the sensitive residues. However, these rules did not apply to the sensitive residues of MnP bound to NP and TCS. The effect of the combination of SWCNT and GRA on the contribution energy of the sensitive residues was comparable to that of single SWCNT or GRA, although some exceptions might occur.

3.3. Water molecular behavior

3.3.1. Water number

Water molecules near MnP and its substrates might have an impact on the binding processes and their binding affinity, because some previous studies have pointed out that the behavior of water molecules was associated with protein function and protein-ligand

interaction (Li and Lazaridis, 2007; Cappel et al., 2011; Chen et al., 2016b). Water number within 5 Å of MnP and within 5 Å of ligands (BPA, NP or TCS) was counted to reveal water-molecule-behavior dynamics along the MnP and its substrates (Fig. 4). This calculation was done for last 10 ns. Note that the initial conditions for all analyzed systems were same. Four cases (SWCNT, GRA, SWCNT+GRA and no nanomaterials) were included for comparison. SWCNT+GRA significantly disturbed the water molecule behavior near MnP and NP as well as MnP and TCS with a decrease of water number (on average by about 77% for MnP and NP; on average by about 71% for MnP and TCS), which implied that SWCNT+GRA prevented some water molecules from penetrating into the region nearby MnP and NP or MnP and TCS; compared to SWCNT+GRA, water molecules in the presence of only single SWCNT or GRA showed less fluctuations in number. By contrast, water molecules number near MnP and BPA increased significantly on average by about 209% in case of single GRA, rather than in cases of SWCNT+GRA or only SWCNT. This may be because the orientation of single GRA is more helpful in moving the water molecules towards MnP and BPA than SWCNT+GRA or single SWCNT.

3.3.2. Contacts of sensitive regions with water molecules

Based on the sensitive residues described above, the regions found to contain one or more sensitive residues in close proximity were identified as sensitive regions. The number of sensitive regions was two for MnP bound to BPA, four for MnP attached to NP, and two for MnP complexed with TCS (Fig. 5).

A previous study investigated the water molecule behavior along the bacteriorhodopsin by GROMACS (Pronk et al., 2013), finding that some key residues formed a dynamic H-bonds network with water molecules (Kandt et al., 2004). In the following we explored the question as to how the sensitive regions took part in the formation of H-bonds with water molecules with or without nanomaterials. As mentioned above, the contribution energy of sensitive residues produced significant fluctuations by the SWCNT, GRA and/or SWCNT+GRA. We wondered whether these fluctuations were partly due to the change of H-bond network formed by water and sensitive residues. Our results showed that the H-bond network for water and sensitive regions was not significantly disturbed by the SWCNT, GRA and/or SWCNT+GRA in all analyzed systems. This implied that the fluctuations of the contribution energy of sensitive residues seemed not to be related to the H-bond network.

3.4. H-bond dynamics of MnP and the substrates with and without nanomaterials

Many previous studies have found that H-bonds played an important role in protein-ligand interaction (Chen et al., 2011, 2015b; Haque and Prabhu, 2014). These H-bonds were crucial in stabilizing the complex of protein with its ligand (Kumar et al., 2014). Thus, H-bond interactions between MnP and the substrates (BPA, NP and TCS) with or without nanomaterials were investigated during the whole simulation based on the donor-

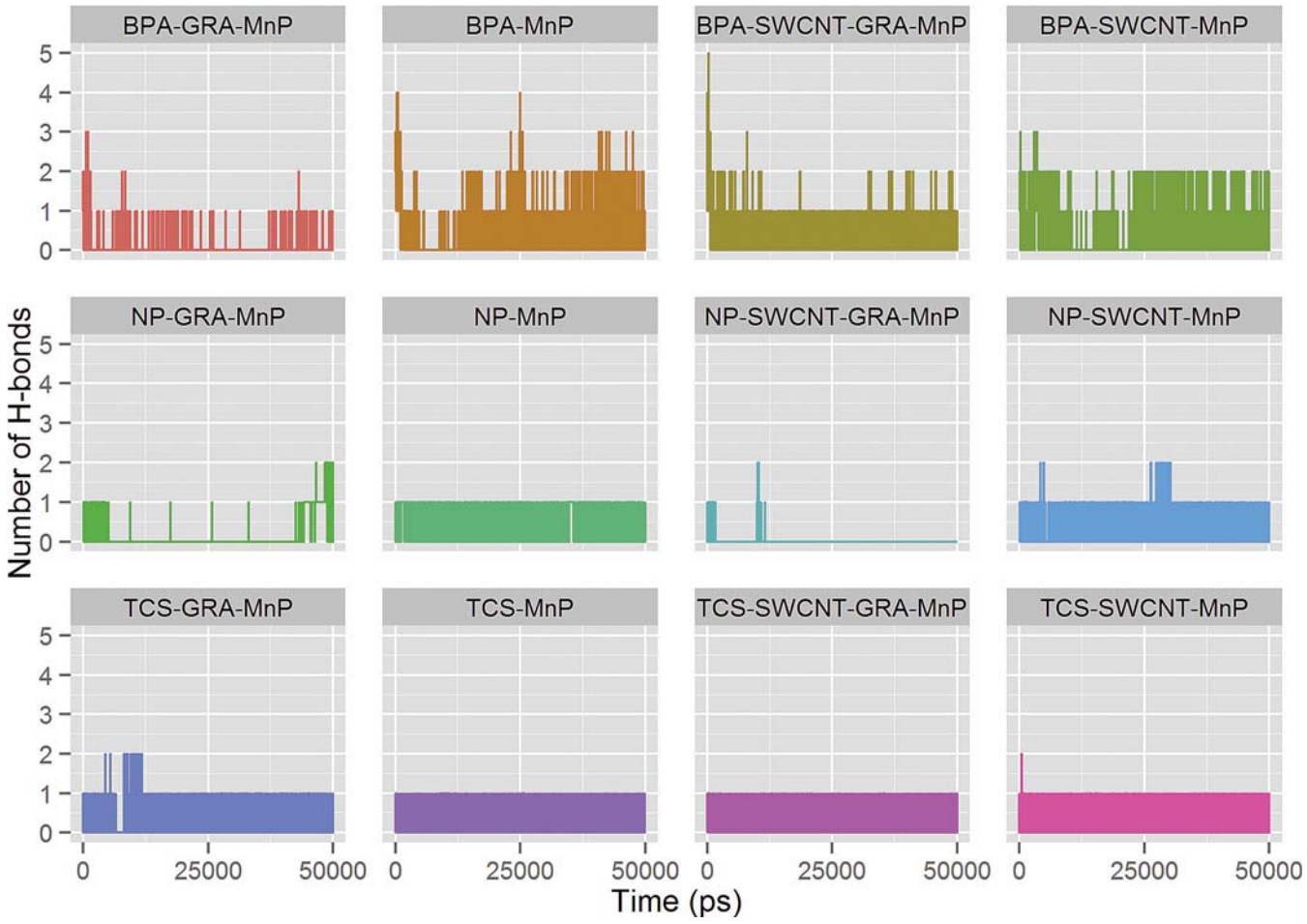

Fig. 6. H-bond dynamics of MnP and the substrates with and without nanomaterials.

acceptor distance and the hydrogen-donor-acceptor angle by g_hbond from GROMACS (Pronk et al., 2013). H-bond dynamics of MnP and the substrates with and without nanomaterials were shown in Fig. 6. For the H-bonds between BPA and MnP, the presence of nanomatirals (SWCNT, GRA or SWCNT+GRA) has changed the H-bonds network. Among these nanomaterials, single GRA tended to inhibit the formation of H-bonds (mean H-bond number: 0.07 for BPA-GRA-MnP and 0.56 for BPA-MnP); in general, the H-bond number was increased at early stage of the simulation but was decreased afterwards in case of SWCNT+GRA; an average number of 0.44 H-bond was observed in the presence of single SWCNT throughout the simulation. MnP exhibited a stable H-bond network with NP in case of no nanomaterials; generally, they maintained one H-bond. This H-bond interaction network often disappeared in cases of GRA or SWCNT+GRA during the whole simulation. In particular, this disappearance time was longer in case of SWCNT+GRA where H-bond was no longer found after about 12 ns. MnP was able to form zero to two H-bond with NP in presence of single SWCNT during the simulation. Interestingly, MnP and TCS with nanomaterials kept a similar H-bond dynamic pattern to those without nanomaterials during the whole simulation, except the early stage with an increase of H-bond number to two. Mean H-bond number was 0.29, 0.36, 0.51 and 0.32 for TCS-MnP, TCS-SWCNT-MnP, TCS-GRA-MnP and TCS-SWCNT-GRA-MnP, respectively.

4. Conclusions

In summary, our results demonstrated that, if a place with EDs and personal care products is polluted by CNTs and/or GRA, their native biodegradation processes may be influenced by these carbon nanomaterials by changing the interactions of the substrates and their enzymes. The most important driving force for the binding between MnP and its substrates were found to be vdW interactions. The single SWCNT or GRA showed different effects on the binding of substrates to MnP due to distinctive properties of these materials. The contribution of each residue to the total binding energy was investigated, indicating that some residues, named “sensitive residues” in this study, were largely disturbed by SWCNT, GRA or their combination. Moreover, the present study further found that the water molecule behavior and H-bond interactions between MnP and the substrates were also changed by these materials. This study helps explore the potential interference of SWCNT, GRA or SWCNT+GRA to biodegradation processes of EDs and triclosan mediated by MnP.

Acknowledgments

The study was financially supported by the National Natural Science Foundation of China (51508177, 51408206, 51521006, 51378190), and the Program for Changjiang Scholars and Innovative Research Team in University (IRT-13R17).

References

Akhavan, O., Ghaderi, E., 2010. Toxicity of graphene and graphene oxide nanowalls against bacteria. Acs Nano 4, 5731–5736.
Anwar, M.A., Panneerselvam, S., Shah, M., Choi, S., 2015. Insights into the species-specific TLR4 signaling mechanism in response to Rhodobacter sphaeroides lipid A detection. Sci. Rep. Uk 5, 7657.
Awasthi, M., Jaiswal, N., Singh, S., Pandey, V.P., Dwivedi, U.N., 2015. Molecular docking and dynamics simulation analyses unraveling the differential enzymatic catalysis by plant and fungal laccases with respect to lignin biosynthesis and degradation. J. Biomol. Struct. Dyn. 33, 1835–1849.
Bhattacherjee, A., Mandal, R.S., Das, S., Kundu, S., 2014. Sequence and 3D structure based analysis of TNT degrading proteins in Arabidopsis thaliana. J. Mol. Model 20, 2174.
Cabana, H., Jiwan, J.-L.H., Rozenberg, R., Elisashvili, V., Penninckx, M., Agathos, S.N., Jones, J.P., 2007a. Elimination of endocrine disrupting chemicals nonylphenol and bisphenol A and personal care product ingredient triclosan using enzyme preparation from the white rot fungus Coriolopsis polyzona. Chemosphere 67, 770–778.
Cabana, H., Jones, J., Agathos, S.N., 2007b. Elimination of endocrine disrupting chemicals using white rot fungi and their lignin modifying enzymes: a review. Eng. Life Sci. 7, 429–456.
Cajthaml, T., 2015. Biodegradation of endocrine-disrupting compounds by ligninolytic fungi: mechanisms involved in the degradation. Environ. Microbiol. 17, 4822–4834.
Calvaresi, M., Hoefinger, S., Zerbetto, F., 2012. Probing the structure of lysozyme-carbon-nanotube hybrids with molecular dynamics. Chem. Eur. J. 18, 4308–4313.
Cappel, D., Wahlström, R., Brenk, R., Sotriffer, C.A., 2011. Probing the dynamic nature of water molecules and their influences on ligand binding in a model binding site. J. Chem. Inf. Model 51, 2581–2594.
Chen, M., Qin, X., Li, J., Zeng, G., 2016a. Probing molecular basis of single-walled carbon nanotube degradation and nondegradation by enzymes based on manganese peroxidase and lignin peroxidase. RSC Adv. 6, 3592–3599.
Chen, M., Qin, X., Zeng, G., 2016b. Single-walled carbon nanotube release affects the microbial enzyme-catalyzed oxidation processes of organic pollutants and lignin model compounds in nature. Chemosphere 163, 217–226.
Chen, M., Qin, X., Zeng, G., 2017a. Biodegradation of carbon nanotubes, graphene, and their derivatives. Trends Biotechnol. http://dx.doi.org/10.1016/j.tibtech.2016.1012.1001.
Chen, M., Xu, P., Zeng, G., Yang, C., Huang, D., Zhang, J., 2015a. Bioremediation of soils contaminated with polycyclic aromatic hydrocarbons, petroleum, pesticides, chlorophenols and heavy metals by composting: applications, microbes and future research needs. Biotechnol. Adv. 33, 745–755.
Chen, M., Zeng, G., Tan, Z., Jiang, M., Li, H., Liu, L., Zhu, Y., Yu, Z., Wei, Z., Liu, Y., Xie, G., 2011. Understanding lignin-degrading reactions of ligninolytic enzymes: binding affinity and interactional profile. Plos One 6, e25647.
Chen, M., Zeng, G., Xu, P., Zhang, Y., Jiang, D., Zhou, S., 2017b. Understanding enzymatic degradation of single-walled carbon nanotubes triggered by functionalization using molecular dynamics simulation. Environ. Sci. Nano 4, 720–727.
Chen, M., Zeng, G.M., Lai, C., Li, J., Xu, P., Wu, H.P., 2015b. Molecular basis of laccase bound to lignin: insight from comparative studies on the interaction of Trametes versicolor laccase with various lignin model compounds. Rsc Adv. 5, 52307–52313.
Fürhacker, M., Scharf, S., Weber, H., 2000. Bisphenol A: emissions from point sources. Chemosphere 41, 751–756.
Feng, Y., Gong, J.-L., Zeng, G.-M., Niu, Q.-Y., Zhang, H.-Y., Niu, C.-G., Deng, J.-H., Yan, M., 2010. Adsorption of Cd (II) and Zn (II) from aqueous solutions using magnetic hydroxyapatite nanoparticles as adsorbents. Chem. Eng. J. 162, 487–494.
Gong, J.-L., Wang, B., Zeng, G.-M., Yang, C.-P., Niu, C.-G., Niu, Q.-Y., Zhou, W.-J., Liang, Y., 2009. Removal of cationic dyes from aqueous solution using magnetic multi-wall carbon nanotube nanocomposite as adsorbent. J. Hazard Mater. 164, 1517–1522.
Haque, N., Prabhu, N., 2014. Insights into protein–TNS (2-p-toluidinylnaphthalene-6-sulfonate) interaction using molecular dynamics simulation. J. Mol. Struct. 1068, 261–269.
Hermanová, S., Zarevúcká, M., Bouša, D., Pumera, M., Sofer, Z., 2015. Graphene oxide immobilized enzymes show high thermal and solvent stability. Nanoscale 7, 5852–5858.
Hess, B., Kutzner, C., van der Spoel, D., Lindahl, E., 2008. Gromacs 4: algorithms for highly efficient, load-balanced, and scalable molecular simulation. J. Chem. Theory Comput. 4, 435–447.
Hirano, T., Honda, Y., Watanabe, T., Kuwahara, M., 2000. Degradation of bisphenol A by the lignin-degrading enzyme, manganese peroxidase, produced by the white-rot basidiomycete, Pleurotus ostreatus. Biosci. Biotechnol. Biochem. 64, 1958–1962.
Huang, D.L., Zeng, G., Feng, C.L., Hu, S., Jiang, X.Y., Tang, L., Su, F.F., Zhang, Y., Zeng, W., Liu, H.L., 2008. Degradation of lead-contaminated lignocellulosic waste by Phanerochaete chrysosporium and the reduction of lead toxicity. Environ. Sci. Technol. 42, 4946–4951.
Humphrey, W., Dalke, A., Schulten, K., 1996. VMD: visual molecular dynamics. J. Mol. Graph 14, 33–38.
Hundt, K., Martin, D., Hammer, E., Jonas, U., Kindermann, M.K., Schauer, F., 2000. Transformation of triclosan by Trametes versicolor and Pycnoporus cinnabarinus. Appl. Environ. Microb. 66, 4157–4160.
Inoue, Y., Hata, T., Kawai, S., Okamura, H., Nishida, T., 2010. Elimination and detoxification of triclosan by manganese peroxidase from white rot fungus. J. Hazard Mater. 180, 764–767.
Kaminski, G.A., Friesner, R.A., Tirado-Rives, J., Jorgensen, W.L., 2001. Evaluation and reparametrization of the OPLS-AA force field for proteins via comparison with accurate quantum chemical calculations on peptides. J. Phys. Chem. B 105, 6474–6487.
Kandt, C., Schlitter, J., Gerwert, K., 2004. Dynamics of water molecules in the bacteriorhodopsin trimer in explicit lipid/water environment. Biophys. J. 86, 705–717.
Kang, J.-H., Katayama, Y., Kondo, F., 2006. Biodegradation or metabolism of bisphenol A: from microorganisms to mammals. Toxicology 217, 81–90.
Kasprzyk-Hordern, B., Dinsdale, R.M., Guwy, A.J., 2009. The removal of

pharmaceuticals, personal care products, endocrine disruptors and illicit drugs during wastewater treatment and its impact on the quality of receiving waters. Water Res. 43, 363–380.
Kim, S., Thiessen, P.A., Bolton, E.E., Chen, J., Fu, G., Gindulyte, A., Han, L., He, J., He, S., Shoemaker, B.A., Wang, J., Yu, B., Zhang, J., Bryant, S.H., 2016. PubChem Substance and Compound databases. Nucleic Acids Res. 44, D1202–D1213.
Kim, Y.-J., Nicell, J.A., 2006. Impact of reaction conditions on the laccase-catalyzed conversion of bisphenol A. Bioresour. Technol. 97, 1431–1442.
Kim, Y., Yeo, S., Song, H.-G., Choi, H.T., 2008. Enhanced expression of laccase during the degradation of endocrine disrupting chemicals in Trametes versicolor. J. Microbiol. 46, 402–407.
Korsman, J.C., Schipper, A.M., de Vos, M.G., van den Heuvel-Greve, M.J., Vethaak, A.D., de Voogt, P., Hendriks, A.J., 2015. Modeling bioaccumulation and biomagnification of nonylphenol and its ethoxylates in estuarine–marine food chains. Chemosphere 138, 33–39.
Kotchey, G.P., Gaugler, J.A., Kapralov, A.A., Kagan, V.E., Star, A., 2013. Effect of antioxidants on enzyme-catalysed biodegradation of carbon nanotubes. J. Mater. Chem. B 1, 302–309.
Kumar, K.M., Anbarasu, A., Ramaiah, S., 2014. Molecular docking and molecular dynamics studies on beta-lactamases and penicillin binding proteins. Mol. Biosyst. 10, 891–900.
Kumari, R., Kumar, R., Lynn, A., Consort, O.S.D.D., 2014. g_mmpbsa-A GROMACS tool for high-throughput MM-PBSA calculations. J. Chem. Inf. Model 54, 1951–1962.
Li, Z., Lazaridis, T., 2007. Water at biomolecular binding interfaces. Phys. Chem. Chem. Phys. 9, 573–581.
Mashiach, E., Schneidman-Duhovny, D., Andrusier, N., Nussinov, R., Wolfson, H.J., 2008. FireDock: a web server for fast interaction refinement in molecular docking. Nucleic Acids Res. 36, W229–W232.
Mubarak, N., Wong, J., Tan, K., Sahu, J., Abdullah, E., Jayakumar, N., Ganesan, P., 2014. Immobilization of cellulase enzyme on functionalized multiwall carbon nanotubes. J. Mol. Catal. B Enzym 107, 124–131.
Omotuyi, I.O., 2015. Ebola virus envelope glycoprotein derived peptide in human Furin-bound state: computational studies. J. Biomol. Struct. Dyn. 33, 461–470.
Pence, H.E., Williams, A., 2010. ChemSpider: an online chemical information resource. J. Chem. Educ. 87, 1123–1124.
Pronk, S., Páll, S., Schulz, R., Larsson, P., Bjelkmar, P., Apostolov, R., Shirts, M.R., Smith, J.C., Kasson, P.M., van der Spoel, D., 2013. GROMACS 4.5: a high-throughput and highly parallel open source molecular simulation toolkit. Bioinformatics 29, 845–854.
Rajesh, C., Majumder, C., Mizuseki, H., Kawazoe, Y., 2009. A theoretical study on the interaction of aromatic amino acids with graphene and single walled carbon nanotube. J. Chem. Phys. 130, 124911.
Rodrigues, D.F., Jaisi, D.P., Elimelech, M., 2013. Toxicity of functionalized single-walled carbon nanotubes on soil microbial communities: implications for nutrient cycling in soil. Environ. Sci. Technol. 47, 625–633.
Rose, P.W., Bi, C., Bluhm, W.F., Christie, C.H., Dimitropoulos, D., Dutta, S., Green, R.K., Goodsell, D.S., Prlić, A., Quesada, M., 2013. The RCSB Protein Data Bank: new resources for research and education. Nucleic Acids Res. 41, D475–D482.
Schneidman-Duhovny, D., Inbar, Y., Nussinov, R., Wolfson, H.J., 2005. PatchDock and SymmDock: servers for rigid and symmetric docking. Nucleic Acids Res. 33, W363–W367.
Sundaramoorthy, M., Gold, M.H., Poulos, T.L., 2010. Ultrahigh (0.93 angstrom) resolution structure of manganese peroxidase from Phanerochaete chrysosporium: implications for the catalytic mechanism. J. Inorg. Biochem. 104, 683–690.
Sundaramoorthy, M., Youngs, H.L., Gold, M.H., Poulos, T.L., 2005. High-resolution crystal structure of manganese peroxidase: substrate and inhibitor complexes. Biochem. Us 44, 6463–6470.
Takamiya, M., Magan, N., Warner, P.J., 2008. Impact assessment of bisphenol A on lignin-modifying enzymes by basidiomycete Trametes versicolor. J. Hazard Mater. 154, 33–37.
Thomsen, R., Christensen, M.H., 2006. MolDock: a new technique for high-accuracy molecular docking. J. Med. Chem. 49, 3315–3321.
Tsutsumi, Y., Haneda, T., Nishida, T., 2001. Removal of estrogenic activities of bisphenol A and nonylphenol by oxidative enzymes from lignin-degrading basidiomycetes. Chemosphere 42, 271–276.
Uguz, C., Iscan, M., Ergüven, A., Isgor, B., Togan, I., 2003. The bioaccumulation of nonyphenol and its adverse effect on the liver of rainbow trout (Onchorynchus mykiss). Environ. Res. 92, 262–270.
Vazquez-Duhalt, R., Marquez-Rocha, F., Ponce, E., Licea, A., Viana, M., 2005. Nonylphenol, an integrated vision of a pollutant. Appl. Ecol. Env. Res. 4, 1–25.
Vidal-Liñán, L., Bellas, J., Salgueiro-González, N., Muniategui, S., Beiras, R., 2015. Bioaccumulation of 4-nonylphenol and effects on biomarkers, acetylcholinesterase, glutathione-S-transferase and glutathione peroxidase, in Mytilus galloprovincialis mussel gilla. Environ. Pollut. 200, 133–139.
Xie, J., Ming, Z., Li, H., Yang, H., Yu, B., Wu, R., Liu, X., Bai, Y., Yang, S.-T., 2016. Toxicity of graphene oxide to white rot fungus Phanerochaete chrysosporium. Chemosphere 151, 324–331.
Xu, P., Zeng, G.M., Huang, D.L., Feng, C.L., Hu, S., Zhao, M.H., Lai, C., Wei, Z., Huang, C., Xie, G.X., 2012. Use of iron oxide nanomaterials in wastewater treatment: a review. Sci. Total Environ. 424, 1–10.
Zhang, Y., Ali, S.F., Dervishi, E., Xu, Y., Li, Z., Casciano, D., Biris, A.S., 2010. Cytotoxicity effects of graphene and single-wall carbon nanotubes in neural phaeochromocytoma-derived PC12 cells. Acs Nano 4, 3181–3186.
Zhang, Y., Zeng, G.-M., Tang, L., Huang, D.-L., Jiang, X.-Y., Chen, Y.-N., 2007. A hydroquinone biosensor using modified core–shell magnetic nanoparticles supported on carbon paste electrode. Biosens. Bioelectron. 22, 2121–2126.
Zhao, J., Wang, Z., White, J.C., Xing, B., 2014. Graphene in the aquatic environment: adsorption, dispersion, toxicity and transformation. Environ. Sci. Technol. 48, 9995–10009.
Zhao, M., Zhang, C., Zeng, G., Huang, D., Xu, P., Cheng, M., 2015. Growth, metabolism of Phanerochaete chrysosporium and route of lignin degradation in response to cadmium stress in solid-state fermentation. Chemosphere 138, 560–567.
Zoete, V., Meuwly, M., Karplus, M., 2005. Study of the insulin dimerization: binding free energy calculations and per-residue free energy decomposition. Proteins 61, 79–93.